THE EFFECT OF CHARGED PARTICLES ON THE POLAR MESOPAUSE REGION, AS OBSERVED BY MST AND METEOR RADARS

A. P. Ballinger[1,*], P. B. Chilson[1], R. D. Palmer[1], S. Kirkwood[2], N. J. Mitchell[3]

[1] School of Meteorology, University of Oklahoma, Norman, Oklahoma, USA
[2] Atmospheric Physics Programme, Swedish Institute of Space Physics, Kiruna, Sweden
[3] Department of Electronic and Electrical Engineering, University of Bath, Bath, UK

Abstract

The decay of meteor trails in the polar mesopause region is thought to be predominantly due to ambipolar diffusion, a process that is governed by the ambient temperature and pressure. However, other processes also play a role, including the absorption of electrons by the numerous charged species that occupy the same region. While the absorption may be relatively small, it can cause a disproportionate reduction in meteor decay time, depending on the initial strength of the meteor trail.

This effect is enhanced in the presence of polar mesospheric summer echoes (PMSE), phenomena arising most probably due to highly charged, sub-visible ice particles that can exist at the extremely cold summer polar mesopause. These charged "dust" particles absorb multiple electrons from expanding, collocated meteor trails.

1. INTRODUCTION

The polar summer mesopause is the coldest region of Earth's atmosphere, and is well known for the existence of two widely studied atmospheric phenomena: noctilucent clouds (NLCs) and polar mesosphere summer echoes (PMSE). NLCs are the better understood feature, the thin clouds forming as water molecules freeze at the extremely low temperatures. PMSE is less understood despite much progress being made over the past decade. PMSE is a radar phenomenon, observed as a dramatic increase in the backscattered power returned from the region slightly below the mesopause, at an altitude of approximately 85km. The complexity of the physics in the middle atmosphere along with the inherent difficulty of taking *in situ* measurements near the mesopause has meant that a full understanding of the theory underlying PMSE still awaits. Nonetheless, using a Mesosphere-Stratosphere-Troposphere (MST) radar these echoes can be clearly observed with good spatial and temporal resolution.

At any location during any given day, many thousands of meteors enter the Earth's upper atmosphere. The frequency of incoming meteors fluctuates but generally follows a well-understood diurnal and seasonal cycle. Most of the meteors ablate as they interact with the increasingly dense air molecules, leaving an ionized plasma trail in their wake. A VHF meteor radar is able to detect these short-lived trails (herein referred to as "meteor echoes"), allowing us to calculate certain useful parameters. At Kiruna (68°N), the heights of the meteor echoes are normally distributed about a mean height of 90km. Since these echoes are observed in the mesopause region, the meteor radar measurements can be used in connection with the MST radar PMSE observations to better understand the physics of this region.

The presence of charged dust and ice particles in the summer mesopause region is thought to be a necessary component of the PMSE environment. If these same charged particles have a noticeable effect on meteor echoes we can move a step closer to better understand the mechanisms responsible for generating and maintaining the PMSE structures.

2. BACKGROUND

2.1. Meteor ablation

As a meteoroid enters Earth's atmosphere it undergoes rapid frictional heating as it interacts with the neutral air molecules. The majority of meteoroids are much smaller than the mean free path of molecules in the upper atmosphere, so the interaction is molecular in nature, and fluid flow effects in the vicinity of the meteoroid are not considered important. This leads to meteor ablation, the process by which meteor atoms are stripped away from the surface of the meteoroid. These atoms have an initial velocity comparable to that of the meteoroid, approximately 11–73 km/s, but undergo many more col-

* *Corresponding author address:* Andrew Ballinger, University of Oklahoma, School of Meteorology, 120 David L. Boren Blvd., Rm 4610, Norman, OK 73072-7307; e-mail: andrewb@ou.edu

lisions with relatively stationary atmospheric molecules, quickly slowing down the ions to the thermal velocities of the environment within less than a millisecond [McKinley, 1961].

The air molecules are assumed to transfer their momentum and energy, but not mass, to the meteoroid. As ablated atoms collide with air molecules, an electron bound to an atom or molecule may absorb sufficient energy to overcome the electric potential that originally confined it. This ionization process leads to the formation of a meteor trail, consisting of positive and negative ions and free electrons, following the path of the meteoroid.

Following Badger [2002], the line density of ablated electrons, q, can be described by the formula

$$q = \frac{\beta C_s}{\mu v}\left(\frac{m}{\rho_m}\right)^{\frac{2}{3}} \frac{K_1 \mathrm{e}^{\frac{K_2}{T}}}{\sqrt{T}}, \tag{1}$$

where β is the probability that a single ablated atom of mass μ produces a free electron on collision. The impinging meteor has a velocity, mass, density and surface temperature given by v, m, ρ_m and T, respectively. The dimensionless factor, C_s, depends on the shape of the meteoroid, and the constants K_1 and K_2 depend on the meteoroid material.

Although (1) describes a useful model for electron production from meteor ablation, it does not fully take into account the effects of heat capacity, thermal conduction and fragmentation of the meteoroid material in the ablation process. For this current analysis it suffices to acknowledge that the meteor ablation process leads to a stream of electrons, with a line density depending on a variety of factors.

2.2. Decay of radio meteor echoes

Consider the idealized case where the radius of a meteor trail is much smaller than the radar wavelength, and the effects of diffusion can be ignored. Further, assume the trail is underdense so that each electron in a meteor trail scatters independently, with a scattering cross-section given by

$$\sigma_e = \frac{\mu_0^2 e^4}{16\pi^2 m^2}, \tag{2}$$

where μ_0, m and e are the magnetic permeability of air, electron mass and electron charge, respectively [Tsutsumi, 1995]. Then, using a conventional radar equation, the power scattered from an individual electron, ΔP_r, is given by

$$\Delta P_r = \frac{P_t G_t G_r \lambda^2 \sigma_e}{64\pi^3 R^4}, \tag{3}$$

where P_t is the transmitted power, R is the range of the meteor, and G_t, G_r represent the antenna gain of the transmitter and receiver, respectively [McKinley, 1961]. Assuming the meteor trail is an infinitely long cylinder, (3) can be integrated over all electrons in the trail, to find that

$$P_r = \frac{P_t G_t G_r \lambda^3 \sigma_e}{128\pi^3 R^3} q^2 \frac{C^2 + S^2}{2}, \tag{4}$$

where C and S are Fresnel integrals of diffraction theory [Badger, 2002].

Assuming ambipolar diffusion is the only mechanism by which the meteor echo decays, the backscattered power will decay from an initial value of P_0 according to

$$P(t) = P_0 \exp\left[-\frac{32\pi^2 D_a t}{\lambda^2}\right], \tag{5}$$

where D_a is the "ambipolar diffusion coefficient", and t is the time after the initial peak power.

Defining a "decay time", $\tau_{1/2}$, as the time taken for the power to drop to half the initial, the ambipolar diffusion coefficient can be estimated from the meteor echo decay time by

$$D_a = \frac{\lambda^2 \ln 2}{16\pi^2 \tau_{1/2}}. \tag{6}$$

This ambipolar diffusion coefficient is also dependent on the atmospheric temperature, T, and pressure, p, through the relation

$$D_a = K_{amb}\frac{T^2}{p}, \tag{7}$$

where K_{amb} is a constant [Jones and Jones, 1990; Jones, 1995; Chilson et al., 1996; Hocking et al., 1997]. Hence, If either T or p is known, the other parameter can be deduced once D_a has been determined from the meteor echo decay times. Other methods have also been developed, primarily to estimate temperature [e.g., Hocking et al., 1997], that do not require observed (or modeled) pressure, but instead rely on the measured vertical profile of meteor decay times.

Each method of temperature estimation from meteors requires the assumption that ambipolar diffusion alone governs the decay of the underdense meteor echoes. Havnes and Sigernes [2005] suggested that this may not always be a valid assumption, and that the absorption of electrons in the meteor trail by charged "dust" particles could be responsible for an overestimate in the ambipolar diffusion coefficient. Holdsworth et al. [2006] have investigated some of the methods of temperature estimation using meteor echo decay times over Antarctica, and see evidence that supports the existence of processes other than just ambipolar diffusion playing a significant role, especially during the summer months.

2.3. Charged particles in the mesopause region

In this report the term “charged particles” will be used to describe the charged species that are quasi-continually present in the mesopause region. These particles arise from a variety of processes that will not all be discussed here, but include ionization from solar radiation, particle precipitation from the lower thermosphere, and the ablation of meteors.

Nearly all of the meteoroids that enter the Earth’s atmosphere ablate before reaching the Earth’s surface, with most of the material evaporating in the region between 80 - 100 km [Hunten et al., 1980]. Rosinski and Snow [1961] showed that this vapor can quickly recondense and form secondary particulate matter. The condensation products along with their immediate descendants through coagulation and sedimentation have been termed “smoke” particles by Hunten et al. [1980].

These particles are thought to provide the nuclei for cloud condensation processes leading to NLCs. It is also clear that the smoke is important in the ion chemistry of the region [Gumbel et al., 2003]. Brasseur and Solomon [1986] discuss the production of metal ions originating from meteors. Part of the ionization occurs during ablation, but most of the charged particles are likely produced by photoionization and charge transfer from species such as O_2^+ and NO^+.

In regions where the temperature is low enough to provide sufficiently high supersaturation, large, hydrated ions are able to form [Gumbel and Witt, 2002]. Such conditions regularly occur in the polar mesopause region during the summer months. These “charged aerosols” are considered to be important in the generation and maintenance of PMSE [Gumbel et al., 2003; Rapp and Lübken, 2004], because they are able to alter the environment in a way that allows structures of free electrons to exist at shorter spatial scales. Some of these hydrated ions in the cold mesopause region are large enough to acquire numerous charges, becoming “multiply charged”.

2.4. Revisiting the ambipolar diffusion assumption

The focus of this analysis will be on the effect that electron-ion recombination, or “absorption”, can have on meteor decay times. By not considering this process, one might inadvertently overestimate the ambipolar diffusion coefficient if the recombination term is significant in removing electrons within a decaying meteor trail. This has important consequences for temperature estimation determined from the ambipolar diffusion coefficient, and thus deserves further investigation.

Havnes and Sigernes [2005] suggested that charged particles should have a more pronounced effect on relatively weak meteor trails, compared to stronger trails. This idea is illustrated conceptually in Figure 1. The top panels simplistically represent cross-sections through initial meteor trails (yellow shading) in an environment consisting of positive ions (blue circles), negative ions (red circles), and free electrons (small yellow circles). Although the meteor trails will also contain many ions, the scatter from ions is negligible compared to that from electrons, due to their significantly greater mass.

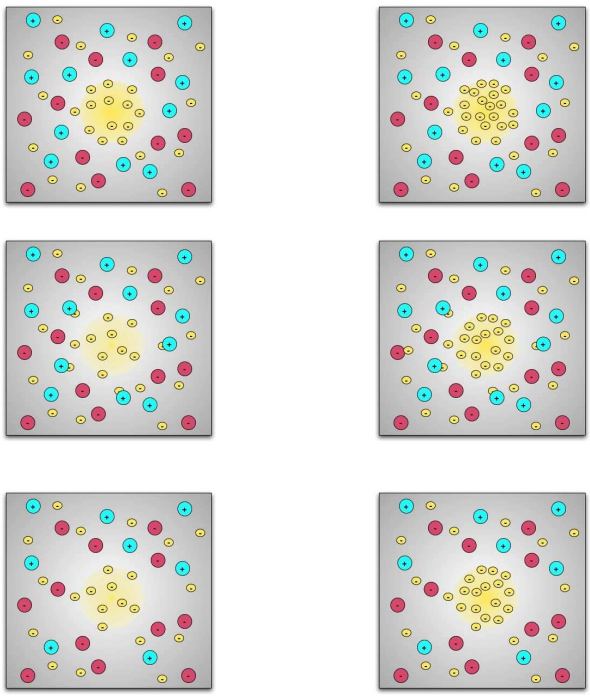

Figure 1: Conceptual illustration showing initial trail (upper panels), ion-electron recombination (middle panels), and adjusted trail (lower panels). Environment consists of positive (blue circles) and negative (red circles) ions, and free electrons (yellow circles). Yellow shading indicates the cross-section of a meteor trail. *Left panels*: Relatively weak initial meteor trail. *Right panels*: Relatively strong initial meteor trail.

The left panel depicts a relatively weaker initial meteor trail, with less electrons contained within the trail radius (lower electron line density) compared to the right panel. Note that the “background” concentration of charged species is the same for both the weak and strong meteors. The middle panels represent the “absorption” process, where a given number of positive ions are available to scavenge electrons diffusing radially outwards

from the trail. In this simple example, a fixed number (four) of positive ions remove the same number of electrons from both the strong a weak trail. After the absorption, the electron densities in each of the meteor trails has been reduced (lower panels). In each case four electrons have been removed, constituting a higher proportion of the initial electrons in the weak trail, compared to the strong.

While simple, this conceptual picture explains the reason why charged particles are expected to have a greater effect on the apparent diffusion of weaker meteor trails. Clearly, for the absorptive effect to be non-negligible, the electron density in the trail cannot be much greater than the electron absorption capability of the dust. Havnes and Sigernes [2005] suggest an electron absorption capability in the vicinity of the center of the meteor trail of the order of 0.1–1% of the initial electron density would be sufficient to cause a reduction in decay time on the order of a few percent.

In the case of PMSE, where cluster ions are more prevalent, one may expect to see an enhancement of this effect. PMSE are thought to be associated with large, sub-visible, hydrated ions, which are able to be multiply charged. Because of their higher charge, these large aerosol particles could potentially have the ability to scavenge multiple numbers of electrons, causing even higher apparent diffusions. Evidence for this scavenging has been seen in electron "biteouts", coincident with regions of PMSE [e.g., Smiley et al., 2003; Havnes et al., 2001].

3. INSTRUMENTATION AND DATA ANALYSIS

3.1. Location

In order to study the characteristics of the polar mesopause region using radar, it was necessary to find a suitable ground site in a polar region. Kiruna, a large town in northern Sweden, just north of the Arctic circle (68°N, 20°E), provided the ideal setting for the collection of data. Esrange (Figure 2) is located approximately 40 km east of Kiruna, and is home to a suite of instruments aimed at providing support to the Swedish Space Corporation's high-class rocket and balloon launching programs. The two instruments used in this project, both stationed at Esrange, were a VHF meteor radar, and a nearly collocated MST radar.

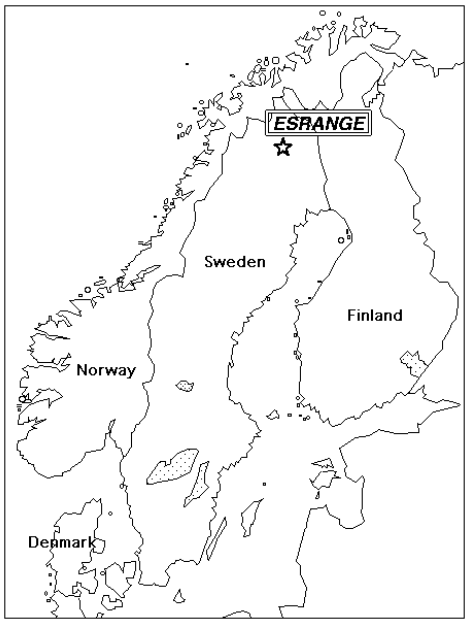

Figure 2: Map of Scandinavia, showing the location of the Esrange facility in northern Sweden. Adapted from a map by `www.EchantedLearning.com`.

3.2. SKiYMET radar

The All-Sky Interferometric Meteor Radar (SKiYMET) system, located at Esrange (Figure 3), is a multi-channel coherent receiver pulsed radar capable of observing a wide range of parameters through the detection and analysis of faint meteors [Genesis, 2002].

The physics underlying the detection of radio-wave scatter from meteor trails was discussed briefly in Section 2.2. As a meteor enters the Earth's atmosphere it heats up and ablates, leaving an ionized stream of plasma in its wake. The meteor radar emits short pulses on its transmit antenna, and measures the received coherent scatter from the individual electrons in the trail on its receive antennas. It follows that the more orthogonal the meteor trail is to direction of propagation, the more easily a coherent reflection from a relatively large length of the trail can occur [Badger, 2002]. This allows fainter trails (lower electron densities) to be observed, and hence, this type of reflection is the most common observed.

The receive antenna array consists of five yagis arranged as an interferometer. When a meteor is detected, a four second window of data is recorded at the detected range, which after signal multiplexing and coherent pulse integration to enhance the signal-to-noise

Figure 3: A photograph of the antenna field of the SKiYMET meteor radar located at Esrange. The radar system comprises five receive antennas, as well as a transmit antenna, covering an area of approximately 2000 m^2.

ratio (SNR) [Hocking et al., 1997], corresponds to approximately 360 in-phase and quadrature pairs per receiver. Cross-correlation functions (CCFs) between all pairs of receiving antennas were found, with the zero time-lag phase enabling standard interferometry procedures [Hocking et al., 1989] to determine the unambiguous angle or arrival [e.g., Hocking et al., 2001; Holdsworth, 2005]. Along with range information, the position of the meteor in the sky can be accurately determined.

The radar transmits at 32.5 MHz ($\lambda = 9.23$ m), with a pulse repetition frequency (PRF) of 2143 kHz (Table 1). A pulse length of 13.3 μs corresponds to a relatively poor range resolution of 2 km, which leads to some ambiguity as to the altitude of any given meteor trail. However, the coarser resolution means that a meteor trail is most likely fully contained within a range gate, which is important in building accurate statistics. So the uncertainty in the height measurement is considered small when averaged over a large number of meteors.

Meteor radar parameters		
Frequency	32.5	MHz
Wavelength	9.23	m
PRF	2143	Hz
Unambiguous range	70	km
Pulse length	13.3	μs
Range resolution	2	km

Table 1: Basic operational parameters employed by the meteor radar.

The PRF leads to an aliasing range of 70 km, however, since most meteors ablate at a height of 90 km ($\pm$20 km), the meteor signals detected are at least second-trip echoes, depending on the zenith angle and range of the individual meteor. Over the course of 2005, more than 3.9 million meteors were observed over Esrange, averaging over 10,000 per day. Over half of these were rejected in order to ensure that only the most reliable meteor signals, and corresponding decay times, were retained (see Ballinger [2007] for details).

3.3. MST radar

The Esrange MST radar (ESRAD) is a sophisticated multiple-receiver 52-MHz radar, primarily used to observe the dynamic state of the atmosphere, from the troposphere to the lower thermosphere (1–110 km altitude). The antenna consists of a 16×18 array of 5-element Yagi antennas, each approximately 6 m high and 3 m across. The antennas are spaced approximately 4 m apart, corresponding to 0.7 times the radar wavelength, with the central 4 Yagis removed to allow for an operations hut (Figure 4).

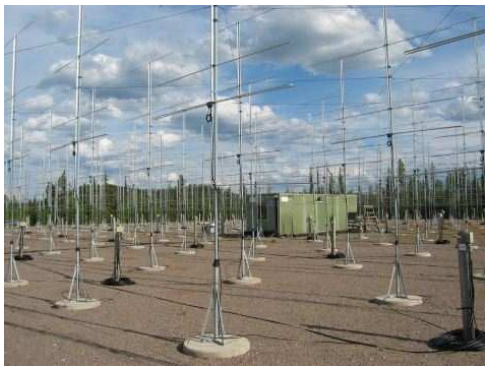

Figure 4: A photograph of the MST radar located in Esrange, Sweden. Some of the individual Yagi antennas are seen, with the control hut located in the center of the array.

The radar transmits at 52 MHz ($\lambda = 5.77$ m), with a PRF for these experiments of 2343 kHz (see Table 2). A pulse length of 1 μs corresponds to a height resolution of 150 m, which is sufficient to resolve most mesospheric echoes. The PRF gives rise to an unambiguous range of 64 km, meaning that mesopause region features (~ 85 km altitude) are clearly within the second-trip echo returns. Hence, in order to isolate the mesopause echoes it is important to differentiate between the signal returned from the first and second trip echoes.

MST radar (ESRAD) parameters		
Frequency	52	MHz
Wavelength	5.77	m
Peak transmit power	72	kW
Maximum duty cycle	4.2	%
Beam width	5	degrees
PRF	2343	Hz
Unambiguous range	64	km
Pulse length	1	μs
Range resolution	150	m

Table 2: Basic operational parameters employed by ESRAD during the experiment.

MST radar waves typically scatter from variations in the refractivity index on scales of half the radar wavelength (Bragg scatter). Such fluctuations arise from sharp gradients in temperature and humidity in the troposphere, and from structures in the free electrons in the upper mesosphere. The lack of moisture, the high thermal stability, and the relatively low transmit power, leads to extremely weak returns from the stratosphere, providing a negligible contribution to the received power. Hence, the tropopause essentially marks the upper range of significant MST power returns, until nearing the ionosphere, where scatter from free electrons (also PMSE in the case of ESRAD), provide significant returns. The height of the tropopause at polar latitudes is generally confined to ~ 10 km [Gabriel et al., 1999], so beyond this height any signal is likely to be associated with the second-trip returns. Specifically in the case of ESRAD, the returns detected at 14–29 km, are "corrected" by the unambiguous range, to give an effective analysis range of 78–93 km, that is centered about the mesopause.

Since the feature of interest to us, PMSE, was a summertime phenomenon, MST data were analyzed for the period from June to August, 2005. Although many different atmospheric properties are diagnosed with MST radar, the variables of interest in the current project were the basic radar outputs: height (range), time, and SNR.

3.4. Analysis of meteor decay times

Since the variation of ambipolar diffusion coefficient with height is important in some methods of temperature estimation, it was useful to construct vertical profiles of decay time. In order to do this it was necessary to determine a representative decay time for each height. The traditional, "arithmetic" mean and standard deviation were not the appropriate measures since the decay times are not normally distributed. However, the distribution is normal for the logarithm transformed values, hence, the "geometric" mean ($\overline{x}$) and standard deviation (σ) can be calculated by

$$\overline{x} = \exp\left[\text{mean}\left(\log X\right)\right] \quad (8)$$

$$\sigma = \exp\left[\text{standard deviation}\left(\log X\right)\right], \quad (9)$$

where X is the log-normally distributed variable [Aitchison and Brown, 1957].

A vertical profile of decay time was constructed by first grouping all incoming meteors over a certain time period into height "bins" of 1 km. This bin width allowed sufficient vertical resolution, while still ensuring a large number of meteors were in each group. The geometric mean decay time and standard deviation of each bin were calculated, and a confidence interval given by

$$\frac{\overline{x}}{\sigma^{\frac{z_{\alpha/2}}{\sqrt{n}}}} < \mu < \overline{x}\sigma^{\frac{z_{\alpha/2}}{\sqrt{n}}}, \quad (10)$$

for a sample of n meteors [Miller and Freund, 1977]. Here, μ represents the actual mean of the distribution, with a $1-\alpha$ probability of lying within the bounds of the confidence interval, and $z_{\alpha/2}$ is such that the area under a normal curve to its right equals $\alpha/2$. For instance, to find the 95% confidence interval ($\alpha = 0.05$) in the position of the mean, one would set $z_{\alpha/2} = 1.96$; for 99% confidence interval ($\alpha = 0.01$), one would set $z_{\alpha/2} = 2.947$ [Miller and Freund, 1977].

The annual mean decay time vertical profile for 2005 is shown in Figure 5. The number of meteors (color shading) reflects the height distribution of incoming meteors, with the majority of meteors falling between 80 km and 100 km. The confidence intervals are not shown since they fall within the thickness of the line that plots the mean decay time profile, indicating the general features of the vertical profile are reliable.

The vertical decay time profile is characterized by a lower maximum at approximately 83 km, with decay time decreasing with altitude above this level, until an upper minimum at approximately 96 km. The meteor decay times throughout this region are assumed to be governed by ambipolar diffusion [e.g., Jones, 1975; Jones and Jones, 1990; Hocking et al., 1997], with decay time being proportional to pressure (decreasing with altitude). The vertical profile of decay time below 83 km, and above 96 km, can be described as "kickback regions", where the decay time appears to increase gently with altitude (for a similar result, see Figure 1 in Hall et al. [2005]). Although the number of meteors is significantly less in these regions, it appears these features are real, and have been briefly discussed by others [e.g., Dyrud et al., 2001; Hall, 2002; Hall et al., 2005].

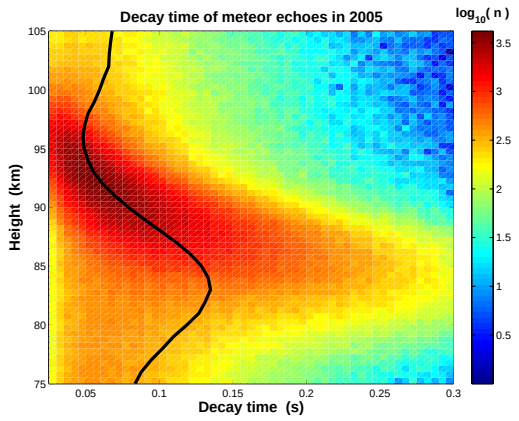

Figure 5: Decay time versus height of all meteors during 2005. Color shading indicates the number of meteors (per 500 m $\times$ 5 msec window). The solid line indicates the mean decay time.

Dyrud et al. [2001] attribute the upper level increase in diffusion (decrease in decay time) to gradient drift Farley-Buneman (GDFB) instability [Fejer et al., 1975], that develops where the trail density gradient and electric field are largest. Above approximately 100 km (perhaps as much as 5 km lower at polar latitudes), collisions dominate ion motion causing them to diffuse out of the trail. The electrons are unable to follow the ions, creating an electric field perpendicular to the meteor trail. GDFB instabilities can grow, leading to anomalous diffusion that exceeds the ambipolar diffusion rate by an order of magnitude [Dyrud et al., 2001]. At lower altitudes (below 96 km), electrons diffuse faster than ions, reversing the electric field and damping any GDFB instability. While the upper "kickback" has important implications for studies that incorporate meteor data from these altitudes, this research has focussed on the mesopause region (below 90 km) where these effects should be negligible.

The reason for the lower "kickback" is more puzzling, with only brief discussion in the literature to date. Hall [2002] acknowledged that this feature is common, and that diffusion only rarely continues to decrease (decay time increase) at altitudes lower than 80–85 km. This is contrary to predictions from ambipolar diffusion theory (Equation 7), suggesting another process (or other processes) contribute at these altitudes. The confidence intervals defining the position of the mean decay time profile are sufficiently narrow to rule out a statistical-averaging effect due to the relatively low number of meteors in this height region.

Hall [2002] suggested that neutral air turbulence may be leading to an overestimation of molecular diffusion, but has subsequently rejected this hypothesis after analyzing new data [Hall et al., 2005]. They suggest other mechanisms that may contribute to the departures, including incorrect meteor altitude determination (from errors in the range and/or zenith angle estimation), and incorrect decay time determination (from inappropriate sampling of individual echoes). It is beyond the scope of the current research to further address this concern, except to acknowledge that the cause(s) of the lower "kickback" may have important ramifications for the use of meteor decay times below this altitude.

The region of interest in this report will be confined to the mesopause region, using vertical profiles, and frequency distributions of meteor data between 80 and 90 km. Although there is confidence in the observed mean decay times within this region, caution is taken not to attribute the decay times below the lower maximum to ambipolar diffusion alone. In fact, it is proposed that at least one other process (electron recombination) has a detectable influence on meteor decay times throughout the mesopause region.

3.5. Combining meteor and MST radar data

To effectively compare the observations from both radars required a method by which each incoming meteor detected by the meteor radar was "matched" to a particular MST observation, both in time and space. Both the temporal (within 3 minutes) and spatial (within 150 m height) matching requirements ensured that meteors detected entering Earth's atmosphere at times when there were no corresponding MST measurements were disregarded for the purpose of data comparison. This enabled further atmospheric information to be added to the meteor database, chiefly the SNR (from the MST radar) as a proxy for the presence of PMSE.

Despite the radars being almost collocated, the method of matching the observations made by each radar in space requires a broad assumption. This arises from the difference in the phenomena being observed. Through interferometric techniques, each meteor has a specific range, zenith, and azimuth angle associated with it, specifying its three-dimensional location. However, the MST radar does not distinguish the direction of signal, rather it "sees" the return signal from the entire area impinged by the transmitted beam.

For each meteor observed, the entire region being observed by the MST radar, at the corresponding height, is assumed to be homogeneous. The SNR observed by

the MST radar is thus assumed to be representative of the SNR in the immediate vicinity of any meteor trail at the corresponding height. Under this assumption each of the summer meteor echoes (June – August) were matched to a corresponding MST derived SNR. These SNR data were then used to ascertain the occurrence or non-occurrence of PMSE. A meteor observed at a certain height (in any direction) is assumed to have ablated in a region of "PMSE" or "No PMSE', as determined by the corresponding MST radar SNR.

Figure 6 illustrates scenarios when this assumption holds true, and other cases when the assumption will inevitably lead to errors. First note that the diagram is obviously not drawn to scale; in reality the two radars are practically collocated, with the distance between them only $\sim 1\%$ of the range to the meteors and PMSE. The meteor labeled 'A' is clearly not within a region of PMSE. However, by assuming areal homogeneity of the SNR detected overhead the MST radar, this method labels the meteor as being associated with a region of PMSE, as it is at the same height. Likewise, meteor 'D' is similarly misdiagnosed as being in a region without PMSE, because of the spatial inhomogeneity at the corresponding height.

The assumption becomes increasingly valid as the meteor zenith angle decreases, since the required areal extent of the uniform echoes effectively reduces. For meteors 'B' and 'C' in Figure 6, at relatively smaller zenith angles, note that the scheme correctly attributes the meteors to regions with and without PMSE, respectively. Certainly, for zenith angles less than $\sim 4.2°$, the beamwidth of the MST radar, it is almost certain that the meteors are collocated with the region of MST return echoes.

PMSEs are typically found at a height of ~ 85 km (± 3 km), so this part of the analysis was restricted to the region between 82–88 km. Meteors corresponding to MST radar observed SNR > 0 dB (signal greater than the noise) were regarded as being *likely* to have ablated in the presence of PMSE, and were hence categorized as "PMSE" meteors. Similarly, those meteors corresponding to MST radar observed SNR ≤ -15 dB (less than the median SNR) were regarded as being *unlikely* to have ablated in the presence of PMSE, and were categorized as "No PMSE" meteors. Figure 7 shows the frequency distribution of the MST radar SNR associated with all incoming meteors (after filtering) for 2005, as well as the distribution for the "PMSE" and "No PMSE" meteors. There were far fewer meteors deemed to be in regions of PMSE compared to those not in PMSE (ratio of approximately 1:10), but this was expected considering the temporal and spatial evolution and variation of PMSE.

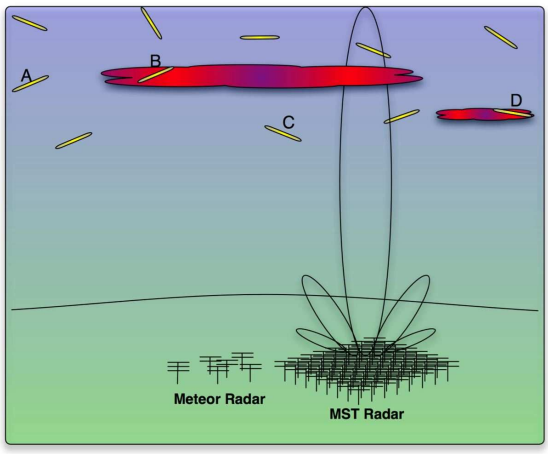

Figure 6: Conceptual diagram outlining the limitations of the areal homogeneity assumption. The meteor and MST radar (with antenna pattern), incoming meteors (yellow lines), PMSE (red regions) are all shown. Four meteor detections are labeled:
Meteor A — Not in PMSE, but designated "PMSE".
Meteor B — In PMSE, and designated "PMSE".
Meteor C — Not in PMSE, and designated "No PMSE".
Meteor D — In PMSE, but designated "No PMSE".

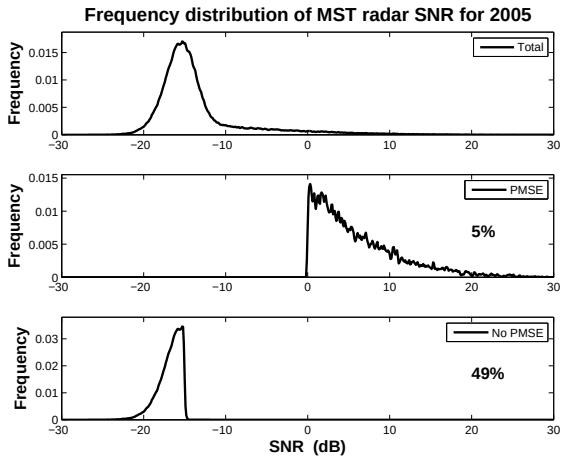

Figure 7: *Upper panel*: Frequency distribution of the MST radar SNR associated with incoming meteors at heights between 82–88 km, during June–August 2005. *Middle panel*: Same as upper panel, but for the meteors likely to be in a region of PMSE (SNR > 0 dB; 5% of the total). *Lower panel*: Same as upper panel, but for the meteors unlikely to be in a region of PMSE (SNR ≤ -15 dB; 49% of the total).

4. RESULTS

4.1. Seasonal variation in meteor echo decay times

Using zonally-averaged mesospheric temperature and pressure at various heights near the mesopause, taken from the CIRA-86 reference atmosphere [Fleming et al., 1990] at 70°N, equations (6) and (7) can be used to qualitatively predict the seasonal cycle of meteor decay time, assuming diffusion by ambipolar processes alone (Figure 8).

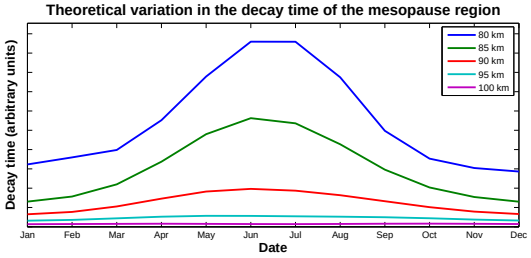

Figure 8: Theoretical seasonal variation in the meteor decay of the mesopause region. Data were taken from the CIRA-86 reference atmosphere (70°N), assuming meteor trail decay by ambipolar diffusion alone.

The actual seasonal variation of meteor decay times is shown in Figure 9, where the daily mean decay times for meteors at heights between 80–90 km are plotted.

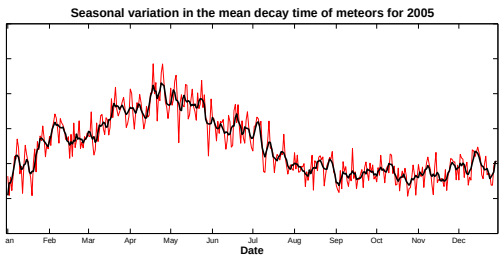

Figure 9: Seasonal variation in the mean decay time of meteors for 2005. The daily mean decay times are shown (thin red line), as well as a 5-day running mean (thick black line).

Although the data show a distinct seasonal cycle, there is a noticeable difference to that predicted by ambipolar diffusion theory alone. Instead of being collocated with the time of minimum temperature, the maximum in decay time is considerably earlier, at the start of May. It is unclear whether this is best described as a seasonal shift in the ambipolar diffusion response to the temperature fluctuations, or some other process is playing a role to reduce decay times, specifically during the summer months. The "seasonal shift" seems least likely, as rather than suggest a lag, it requires the ambipolar diffusion response to pre-empt the temperature fluctuations by at least a month or two. Considering the molecular nature of ambipolar diffusion, this explanation seems almost inconceivable. It would appear that some other process or processes are reducing decay times preferentially in the summer months.

Height-dependent effects that might be missed when only viewing an average over a height range cannot be ruled out. Hence, the seasonal variation of the vertical profile of meteor decay times is investigated. A slight variant of Figure 8 is shown in Figure 10, once again using the CIRA-86 reference atmosphere. Plotted are the theoretical vertical profiles of the monthly averaged decay time (qualitative) for the mesopause region, once again assuming ambipolar diffusion governs the decay. The cooler summer months imply slower diffusion and hence, longer decay times.

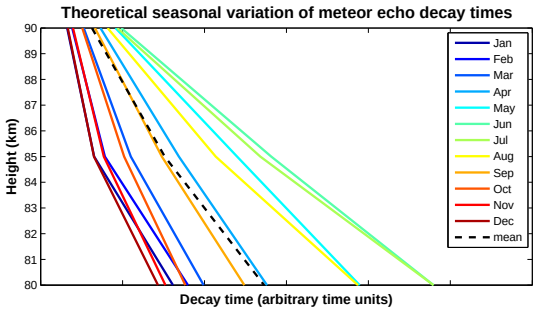

Figure 10: Theoretical vertical profiles of the monthly-averaged decay time derived using the CIRA-86 reference atmosphere conditions at 70°N. The dashed line indicates the annual mean.

The actual vertical profiles of mean meteor decay time are shown in Figure 11. The left panel shows the monthly mean decay time profiles, with the right panel indicating the difference from the annual mean decay time profile. Note that at higher altitudes the decay time is consistent with the qualitative prediction shown in Figure 10. However, looking at the lower levels, notice the departure from that which is expected with ambipolar diffusion, particularly in the case for the summer months (June–August). Indeed, more needs to done to understood the lower "kickback" and the processes that determine its position and seasonal variation. Nonetheless, the reduction in decay time during the summer months is disproportionately large, and deserves further investigation.

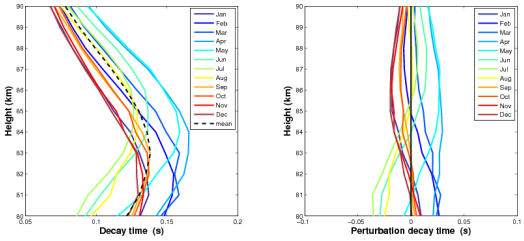

Figure 11: *Left panel*: Vertical profiles of the monthly mean decay time of meteor trails for 2005. The dashed line indicates the annual average of the monthly mean decay times. *Right panel*: Vertical profiles of the perturbation decay time, defined as the difference between the monthly and annually averaged decay time.

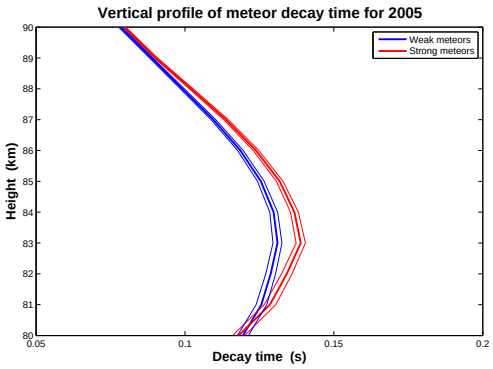

Figure 12: Vertical profiles of mean decay time for 2005. The profile of weak meteors ($\mathrm{SNR} < 12$ dB) is shown in blue; strong meteors ($\mathrm{SNR} \geq 12$ dB) in red. The thin lines either side of the mean profiles indicate the 99% confidence interval bounds.

4.2. Evidence for background charged particles

In order to compare weak and strong meteor echoes, the incoming meteors were divided into two groups of approximately the same number, based on the initial trail strength (SNR). Meteor echoes with SNR < 12 dB are termed *weak*, while echoes with SNR ≥ 12 dB are termed *strong*. Note that this is not an absolute categorization, but rather a method of dividing the total echoes into approximately equal numbers of "relatively weaker" and "relatively stronger" meteor echoes. As per the stated hypothesis, the initially weaker echoes should be more affected by the presence of charged particles.

The mean profile of decay time for incoming meteors during 2005, constructed for both weak ($\mathrm{SNR} < 12$ dB) and strong ($\mathrm{SNR} \geq 12$ dB) meteor trails is shown in Figure 12. The thin lines represent the bounds of the mean within a 99% confidence interval. A significant reduction in decay time is evident throughout the range ~82–88 km, with a maximum reduction of approximately 0.01 s ($\sim 10\%$) at 83 km.

The frequency distribution of decay time for weak and strong meteors for incoming meteors at heights between 80 km and 90 km is shown in Figure 13. There appears to be a pronounced shift towards lower decay times for the weaker echoes. This reduction is apparent across most decay times, showing little evidence for reducing short or long decay times preferentially. These findings support the suggestions made by Havnes and Sigernes [2005] who stated that a discovery of shorter decay times for weaker echoes gives evidence towards the existence of charged particles in the mesopause region.

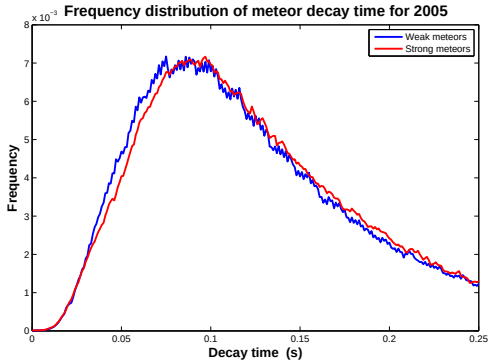

Figure 13: Frequency distributions of meteor decay times for 2005. The distribution of weak meteors ($\mathrm{SNR} < 12$ dB) is shown in blue; strong meteors ($\mathrm{SNR} \geq 12$ dB) in red.

It is useful to see if the seasonal cycle of decay time (discussed in Section 4.1) can shed light on some on the processes affecting weak and strong meteor echoes. Figure 14 shows three-monthly averages of the mean decay time vertical profiles for the strong and weak meteors.

Note that the weaker trails have a consistently shorter decay time, throughout the year, providing evidence of the yearly charged state of the mesopause region. However, the extent of this reduction appears to vary seasonally, with the most pronounced absorption being in the first and fourth quarters when the "kickback" is at lower altitudes. In fact, chiefly during the April–June quarter when the maximum in decay time is at the highest alti-

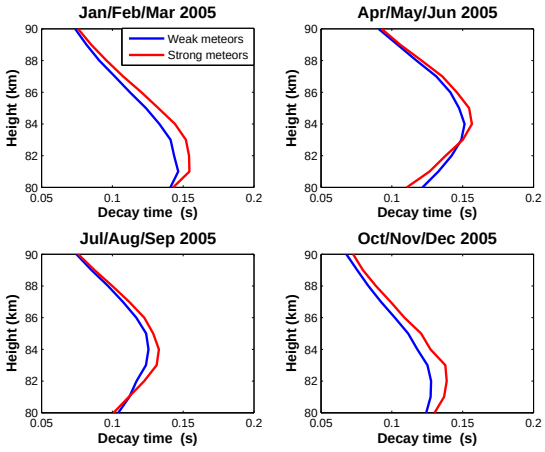

Figure 14: Seasonal variation in mean decay time vertical profiles for 2005. The profiles of weak meteors ($\mathrm{SNR} < 12$ dB) are shown in blue; strong meteors ($\mathrm{SNR} \geq 12$ dB) in red. January–March (upper left), April–June (upper right), July–September (lower left), and October–December (lower right).

tude, the stronger meteors actually have a lower mean decay time at altitudes below this point. As discussed in Section 3.4, the processes occurring below the height of maximum decay time are poorly understood and clearly deserve more investigation. While beyond the scope of this report, future work is needed to isolate the dominant processes of this region. However, the question remains as to why, even above the "kickback", there appears to be a significantly smaller reduction in meteor decay time due to the presence of charged ions during the summer months, when it is during these months that ionization levels are the greatest.

4.3. Evidence for charged aerosols associated with PMSE

Vertical profiles of mean decay time were constructed for both the "PMSE" and "No PMSE" meteors (Figure 15) during the 2005 summer months. Note that the 95% confidence intervals are relatively large, especially in the case of the "PMSE" meteors , reflecting the lower sample size from which the mean is determined.

Nonetheless, there is a noticeable reduction in decay time over the small region centered on the peak of the PMSE distribution. This demonstrates that those meteors likely within PMSE are being absorbed by charged particles. Furthermore, since background charged species are quasi-uniformly spread throughout this region, and should affect all meteors, it is proposed that the reduction seen in the PMSE meteors is an enhancement to the regular absorption (discussed in Section 4.2), and is caused by large dust particles that have been charged multiple times.

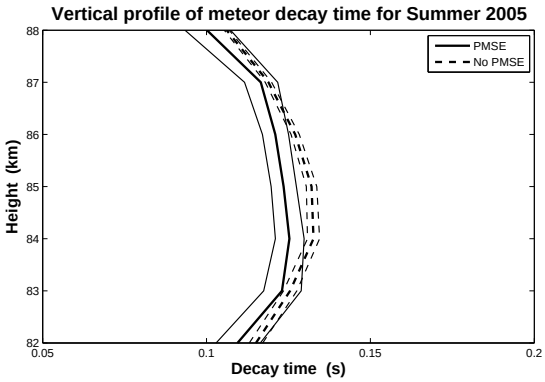

Figure 15: Vertical profiles of mean decay time during summer 2005, showing the profile for "PMSE" meteors (solid line), and "No PMSE" meteors (dashed line). The thin lines either side of the mean profiles indicate the 95% confidence interval bounds.

5. CONCLUSIONS

Charged particles, existing semi-permanently in the mesopause region, have a marked effect on meteor decay times, forcing a re-examination of the ambipolar diffusion assumption. Processes, such as electron absorption, should not be ignored, especially in the case of weaker meteors or meteors associated with PMSE. If not taken into account, the ambipolar diffusion coefficient can be overestimated. Hence, caution must be taken when retrieving mesopausal temperatures using meteor decay times. Used in conjunction with a modeled pressure, an overestimate in ambipolar diffusion coefficient can lead to an overestimate in the temperature.

These results lead to a better understanding of the mesopause region. Rockets have previously been the only tool capable of observing the charged species in the mesopause region, having the severe limitation of being restricted to small spatial and temporal sampling. Being able to indirectly observe the presence of positively charged particles by their effect on meteor decay times opens up an entirely new realm of opportunities for investigating the microphysical nature of this unique region. With speculation still surrounding the way PMSE is generated and maintained, this technique adds another line of evidence to support the importance

of highly charged particles. Furthermore, with meteor data continually available throughout the year, greater understanding into the seasonal and diurnal variations of the mesopause region may be possible.

References

Aitchison, J., and J. A. C. Brown, 1957: *The lognormal distribution*. Cambridge University Press, Cambridge.

Badger, D., 2002: *Fine structures in radio meteor showers*. PhD Thesis, University of Adelaide.

Ballinger, A., 2007: *Radio-wave scatter and dynamical processes in the polar mesopause region observed using MST and meteor radars*. M.S. Thesis, University of Oklahoma.

Brasseur, G., and S. Solomon, 1986: *Aeronomy of the middle atmosphere*. D. Reidel Publishing Company, Dordrecht, Holland, second edition.

Chilson, P. B., P. Czechowsky, and G. Schmidt, 1996: A comparison of ambipolar diffusion coefficients in meteor trains using VHF radar and UV lidar. *Geophys. Res. Lett.*, **23**, 2745–2748.

Dyrud, L. P., M. M. Oppenheim, and A. F. vom Endt, 2001: The anomalous diffusion of meteor trails. *Geophys. Res. Lett.*, **28**, 2775–2778.

Fejer, B. G., D. T. Farley, B. B. Balsley, and R. F. Woodman, 1975: Vertical structure of the VHF backscattering region in the equatorial electrojet and the gradient drift instability. *J. Geophys. Res.*, **80**, 1313.

Fleming, E. J., S. Chandra, J. J. Barnett, and M. Corney, 1990: Zonal mean temperature, pressure, zonal wind and geopotential height as a function of latitude. *Adv. Space Res.*, **10**, 11–59.

Gabriel, A., G. Schmitz, and R. Geprägs, 1999: The tropopause in a 2D circulation model. *J. Atmos. Sci.*, **56**, 4059–4068.

Genesis, 2002: *SKiMET Meteor Radar Reference Manual (Version 1.8)*. Genesis Software Pty Ltd, North Adelaide, Australia.

Gumbel, J., D. E. Siskind, G. Witt, K. M. Torkar, and M. Friedrich, 2003: Influences of ice particles in the ion chemistry of the polar summer mesosphere. *J. Geophys. Res.*, **108**(D8), doi:10.1029/2002JD002413.

Gumbel, J., and G. Witt, 2002: Cluster ions and ice particle nucleation: Positive feedback at the summer mesopause. *Geophys. Res. Lett.*, **29**(16), doi:10.1029/2002GL015146.

Hall, C. M., 2002: On the influence of neutral turbulence on ambipolar diffusivities deduced from meteor trail expansion. *Ann. Geophy.*, **20**, 1857–1862.

Hall, C. M., T. Aso, M. Tsutsumi, S. Nozawa, A. Manson, and C. E. Meek, 2005: Testing the hypothesis of the influence of neutral turbulence on the deduction of ambipolar diffusivities from meteor trail expansion. *Ann. Geophy.*, **23**, 1071–1073.

Havnes, O., T. Aslaksen, and A. Brattli, 2001: Charged dust in the Earth's middle atmosphere. *Phys. Scripta*, **T89**, 133–137.

Havnes, O., and F. Sigernes, 2005: On the influence of background dust on radar scattering from meteor trails. *J. Atmos. Sol.-Terr. Phys.*, **67**, 659–664.

Hocking, W. K., B. Fuller, and B. Vandepeer, 2001: Real-time determination of meteor-related parameters utilizing modern digital technology. *J. Atmos. Sol.-Terr. Phys.*, **63**, 155–169.

Hocking, W. K., P. May, and J. Röttger, 1989: Interpretation, reliability and accuracies of parameters deduced by the spaced antenna method in middle atmosphere applications. *Pure Appl. Geophys.*, **130**, 571–604.

Hocking, W. K., T. Thayaparan, and J. Jones, 1997: Meteor decay times and their use in determining a diagnostic mesospheric temperature-pressure parameter: Methodology and one year of data. *Geophys. Res. Lett.*, **24**, 2977–2980.

Holdsworth, D. A., 2005: Angle of arrival estimation for all-sky interferometric meteor radar systems. *Radio Sci.*, **40**(RS6010).

Holdsworth, D. A., R. J. Morris, D. J. Murphy, I. M. Reid, G. B. Burns, and W. J. R. French, 2006: Antarctic mesospheric temperature estimation using the Davis mesosphere-stratosphere-troposphere radar. *J. Geophys. Res.*, **111**(D5), doi:10.1029/2005JD006589.

Hunten, D. M., R. P. Turco, and O. B. Toon, 1980: Smoke and dust particles of meteoric origin in the mesosphere and stratosphere. *J. Atmos. Sci.*, **37**, 1342–1357.

Jones, J., 1975: On the decay of underdense radio meteor echoes. *Mon. Not. R. Astron. Soc.*, **173**, 637–647.

Jones, W., 1995: The decay of radar echoes from meteors with particular reference to their use in the determination of temperature fluctuations near the mesopause. *Ann. Geophy.*, **13**, 1104–1106.

Jones, W., and J. Jones, 1990: Ionic diffusion in meteor trains. *J. Atmos. Terr. Phys.*, **52**, 185–191.

McKinley, D. W. R., 1961: *Meteor Science and Engineering*. McGraw-Hill, New York.

Miller, E., and J. E. Freund, 1977: *Probability and statistics for engineers*. Prentice-Hall, Inc., New Jersey, second edition.

Rapp, M., and F. J. Lübken, 2004: Polar mesosphere summer echoes (PMSE): Review of observations and current understanding. *Atmos. Chem. Phys.*, **4**, 2601–2633.

Rosinski, J., and R. H. Snow, 1961: Secondary particulate matter from meteor vapors. *J. Atmos. Sci.*, **18**, 736–745.

Smiley, B., S. Robertson, M. Horanyi, T. Blix, M. Rapp, R. Latteck, and J. Gumbel, 2003: Measurement of positively and negatively charged particles inside PMSE during MIDAS SOLSTICE 2001. *J. Geophys. Res.*, **108**(D8), doi:10.1029/2002JD002425.

Tsutsumi, M., 1995: *A study of atmospheric dynamics near the mesopause using radio meteor echoes*. PhD Thesis, Kyoto University.